Supporting Information

Huang et al. 10.1073/pnas.0909644106

SI Text

Control Experiments. Extensive control experiments, including protein and DNA binding, FCS, and time-resolved fluorescence anisotropy, were carried out to test for possible structural and functional effects of the mutations and labeling modifications that might have influenced the conclusions derived from the FRET experiments.

Functionality and Structure of Labeled Protein. To look for any influence of the dye labels on the properties of p53, we checked whether the binding affinities of the labeled NTD with Mdm2 and Taz2 proteins were appreciably affected. AF488/AF647 doubly labeled p53N10C56C had dissociation constants of 200 and 25 nM with Mdm2 and Taz2, respectively, which were very similar to those for unlabeled p53 NTD peptides (160 and 27 nM with Mdm2 and Taz2, respectively) (1). The dissociation constant of the AF488-labeled protein with consensus response element DNA (5′ AF647-TGAGGAACATGTCCCAACAT-GTTGAGCTC 3′) was 60 nM for flp5356C229C, which was similar to that for wild-type p53 with the same DNA (2). The control experiments suggest that the dyes had little effect on the protein functionality and structure.

FCS. To exclude the possibility that the multiple peaks in the SM-FRET efficiency histogram were caused by aggregation of proteins, we measured the diffusion time of the p53 mutants with FCS. The experiments were carried out with a confocal fluorescence microscope similar to that used for the single-molecule FRET experiments under the same conditions but with 10 nM labeled protein. Typical FCS decay curves are shown in Fig. S2. The diffusion time for different mutants varies between 0.2 and 0.6 ms (an acceptable range). No extraordinarily slow diffusing species were observed in all cases, suggesting that there were no aggregates in the samples.

Time-Resolved Anisotropy Experiments. Fluorescence anisotropy decays were recorded by using time-correlated single photon counting techniques as described (3–6). Excitation of the donor was achieved by using a picosecond amplified and frequency doubled diode laser (490-nm, 100-ps pulse width) operating at 5 MHz (PicoTA). Excitation of the acceptor at 615 nm was undertaken by using the pulse-picked output (3.8 MHz, sub 1 ps) of an optical parametric oscillator (Coherent Mira), synchronously pumped by a 76-MHz mode locked Ti:Sapphire laser (Mira 900F and Verdi V10; Coherent). Fluorescence measurements were carried out at ≈2 μM concentrations at room temperature (21–22 °C) in 50 μL of quartz fluorescence cuvettes (Hellma). Fluorescence was detected by a microchannel plate photomultiplier (R3809U; Hamamatsu), using a right-angled excitation-detection geometry with the appropriate choice of filters. For donor fluorescence measurements, a 531 ± 11-nm band pass filter (Semrock) was used. Acceptor fluorescence was detected through an OG530 and RG665 long pass filter combination. A quartz Glan Taylor polarizer (Karl Lambrecht) was used to produce vertically polarized (0°) excitation pulses. An analyzing sheet polarizer (CVI-Melles) was sequentially altered between 0° (vertical, V) and 90° (horizontal, H) to obtain the polarized intensity measurements $I_V(t)$ and $I_H(t)$, here t denotes the excitation–detection coincidence time measured by the TCSPC system. The fluorescence intensities $I(t)$ and emission anisotropies $r(t)$ were determined from $I(t) = I_V(t) + 2I_H(t)$ and $r(t) = (I_V(t) - I_H(t))/(I_V(t) + 2I_H(t))$, respectively.

Time-resolved fluorescence anisotropy decays were measured for all of the mutants by exciting the donor and observing the emission of the donor and the acceptor or by exciting the acceptor directly and observing the emission of the acceptor. To determine the behavior of the fluorescence anisotropy of the donor in the absence of FRET, two donor-only labeled p53 mutants were also studied. One mutant was labeled at position 56 and the other labeled at position 229. These mutants have only one exposed cysteine at position 56 or 229, respectively. All of the mutants show a biexponential anisotropy decay with a very fast component (<1 ns) and a relatively slow decay (≈3–10 ns) (see Fig. S3). The slow components in the time-resolved anisotropy decay were hard to determine accurately because of the short fluorescence lifetimes (≈2 ns) and therefore contain relatively large errors. The fast decay component can be attributed to the fast local rotation of the bound fluorophores and the slow decay represents the segmental flexibility or the tumbling of the protein as a whole. The amplitude of the fast components is indicative that both donor and acceptor molecules are free to undergo significant internal orientational relaxation and that it is reasonable to assume the κ^2 to be 2/3 in the calculation of Förster distance (7, 8). This also indicates that the multiple peaks in the single-molecule FRET efficiency histogram do not arise from restricted fluorophores, as reported in previous work for a different system (9). It is also notable that the fluorescence anisotropy for all of the mutants has decayed to zero within ≈25 ns, which further supports the absence of aggregates in the sample.

TR-FRET Data Analysis. The time-resolved FRET data were fitted to Eq. **1** numerically:

$$\frac{\partial}{\partial t} g_{\mathrm{N}}^{*}(r,\,t) = -\frac{1}{\tau_0}\left(1 + \left(\frac{R_0}{r}\right)^6\right) g_{\mathrm{N}}^{*}(r,\,t) + D\,\frac{1}{r^2}\frac{\partial}{\partial r}\,r^2\,\frac{\partial}{\partial r}\,g_{\mathrm{N}}^{*}(r,\,t) + D\,\frac{1}{r^2}\frac{\partial}{\partial r}\left(r^2 g_{\mathrm{N}}^{*}(r,\,t)\,\frac{\partial}{\partial r}\,\beta U(r)\right), \qquad [1]$$

where D is the mutual intramolecular end-to-end diffusion constant, the sum of the diffusion coefficients of the two ends. β^{-1} is the product of the Boltzman constant and temperature ($\beta = 1/k_{\mathrm{B}}T$), and $U(r)$ is the potential energy of the chain possessing an end-to-end distance r. If the ground-state equilibrium radial distribution function $g_N(R)$ is known, the potential energy can be obtained according to Eq. **2**, assuming no perturbation of the distribution function upon excitation of the donor (8, 10).

$$\beta U(r) = -\ln g_{\mathrm{N}}(r). \qquad [2]$$

Eq. **1** can be used to calculate the survival probability density of an excited state at distance r subject to the boundary conditions:

$$\frac{\partial}{\partial r} g_N^{*}(r,\,t) + g_N^{*}(r,\,t)\,\frac{\partial}{\partial r}\,\beta U(r)\Big|_{r=r_{\min}} = 0 \qquad [3a]$$

$$\frac{\partial}{\partial r} g_N^{*}(r,\,t) + g_N^{*}(r,\,t)\,\frac{\partial}{\partial r}\,\beta U(r)\Big|_{r=r_{\max}} = 0 \qquad [3b]$$

In the present work TR-FRET data were fitted assuming a normally distributed $g_N(R)$:

$$g_N(r) = \frac{1}{\sigma\sqrt{2\pi}} \exp\left(-\frac{(r - r_0)^2}{2\sigma^2} \right). \quad [4]$$

Thus, the free parameters of the fit are r_0, σ, and D. For each trial set of parameters, the differential Eq. **1** was solved numerically, using the boundary conditions in Eq. **3**.

The Gaussian chain model (or random coil model) has also been used for comparison. In that case the radial distribution function is:

$$g_N(r) = \left(\frac{3}{2\pi\sigma^2} \right)^{3/2} \exp\left(-\frac{3(r)^2}{2\sigma^2} \right). \quad [5]$$

The theoretical fluorescence decay was convoluted with the experimental instrument response function and compared with experimental data. The least-squares fit was accomplished by minimizing the mean squared deviation (χ^2) between time-resolved FRET data and the theoretical model using the Levenberg-Marquardt algorithm. The error on the parameters was assigned by using the projections of the region of parameter space where $\chi^2 < 1.05\times \chi^2_{\min}$. The latter was sampled by using a Monte-Carlo procedure in the parameter space with χ^2 as energy function, and temperature and step size allowing a 30% acceptance ratio.

Calculation of Förster Critical Distance. The Förster critical distance, R_0, was calculated for each FRET pair with Eq. **6**:

$$R_0 = 0.211[\kappa^2 n^{-4} Q_D J]^{1/6}, \quad [6]$$

where κ^2 is the dipole orientation factor and assumed to be 2/3; n is the refractive index of the solution measured experimentally; Q_D is the fluorescence quantum yield of the donor and obtained from the donor-labeled protein, with reported fluorescence quantum yield from Invitrogen for corresponding free dye as reference; J is the overlap of the emission spectrum of the protein-labeled donor and the absorption spectrum of the protein-labeled acceptor. Dyes labeled on p53NCD(56C91C) and flp53(56C229C) were used to calculate the Förster critical distances. Owing to very similar fluorescence quantum yields and spectra obtained for dyes labeled on these two protein constructs, the same R_0 values within error were obtained. The Förster distance for Nal/EDANS was calculated with fluorophores labeled in the p53N1–17 peptide and assumed to be the same for the other two peptides with the same pair. The Förster distance for EDANS/Dabcyl was based on the fluorophores labeled in the p53N14–30 peptide.

Data Analysis for SM-FRET Experiments. FRET efficiencies (E) of each burst were calculated according to $E = (n_A)/(n_A) + \gamma n_D)$, where n_A, and n_D are the background corrected photon counts from the acceptor and donor, respectively, and γ is the constant to correct the difference in fluorescence quantum yield of the donor and acceptor and the detection efficiency of the detectors for the donor and acceptor. For the used FRET pairs and the current setup, $\gamma \approx 1$. To calculate the γ value, the fluorescence quantum yield of the labeled dyes was measured and the relative detection efficiency of the donor and acceptor channels was determined by comparing the FRET efficiency of DNA sample labeled with the same donor/acceptor pair with 100% labeling efficiency obtained from the confocal setup and a calibrated fluorometer. The peak position of the histogram with single peak was determined by fitting the histogram with a double skewed Gaussian distribution

$$\left(y = A_1 \exp\left(-\frac{(x - x_1)^2}{2\sigma_1^2} \right) + A_2 \exp\left(-\frac{(x - x_2)^2}{2\sigma_2^2} \right) + C \right),$$

for the zero peak and the real FRET peak.

Distance Calculation for Steady-State FRET Experiments. The FRET in the AF488/ReAsH system was determined by steady-state fluorescence intensity, i.e., $E = (I_D - I_{DA})/I_D$, where E, I_D, and I_{DA} are the FRET efficiency, fluorescence intensity of AF488 in the absence and presence of ReAsH, respectively. The distance between dyes (r) was then calculated with $r = (1/E - 1)^{1/6} R_0$.

Peptide Synthesis. Peptides p53N1–17 [residues 1–17: (Asp-EDANS)-MEEPQSDPSVEPPLSQE-(Nal-Ala)], p53N14–30 [residues 14–30: (Asp-EDANS)-LSQETFSDLWKLLPENN-(Dabcyl-Lys)], p53N62–78 [residues 62–78: (Asp-EDANS)-EAPRMPEAAPPVAPAPA-(Nal-Ala)], and p53N74–92 [residues 74–92: Asp-EDANS)-APAPAAPTPAAPAPAPS-(Nal-Ala)-P)] were synthesized on a Pioneer peptide synthesizer (Applied Biosystems) using standard Fmoc chemistry. Nal-Ala, EDANS, and Dabsyl were incorporated into the peptides during solid-phase peptide synthesis using Fmoc-1-Nal-OH, Fmoc-Asp(EDANS)-OH and Fmoc-Lys(Dabsyl)-OH (all from Bachem), respectively. All other amino acids were purchased from NOVAbiochem. The peptides were purified on a Waters HPLC using a reverse-phase C8 semipreparative column (Vydac) as described (11). All of the peptides were lyophilized and had a purity of >95%.

Protein–Protein and Protein–DNA Binding. To measure the binding constant of NTD of p53 with MDM2 and Taz2, we added MDM2 or Taz2 to 10 nM AF488-labeled NTD. The fluorescence anisotropy was plotted versus titrant concentration, and fitted to a 1:1 binding model (1). The determination of p53-DNA binding constants were carried out as described for dsDNA labeled with AF488 (2).

Circular Dichroism Measurements. Circular dichroism spectra of the peptides were acquired in phosphate buffer (20 mM phosphate plus 100 mM NaCl, pH 7) at concentration ranging from 20 to 40 μM on a J-815 CD Spectrometer (JASCO). The CD spectra are shown in Fig. S4.

1. Teufel DP, Freund SM, Bycroft M, Fersht AR (2007) Four domains of p300 each bind tightly to a sequence spanning both transactivation subdomains of p53. *Proc Natl Acad Sci USA* 104:7009–7014.
2. Weinberg RL, Veprintsev DB, Fersht AR (2004) Cooperative binding of tetrameric p53 to DNA. *J Mol Biol* 341:1145–1159.
3. Bain AJ, Chandna P, Butcher G, Bryant J (2000) Picosecond polarized fluorescence studies of anisotropic fluid media. II. Experimental studies of molecular order and motion in jet aligned rhodamine 6G and resorufin solutions. *J Chem Phys* 112:10435–10449.
4. Marsh RJ, Armoogum DA, Bain AJ (2002) Stimulated emission depletion of two-photon excited states. *Chem Phys Lett* 366:398–405.
5. White SS, et al. (2006) Characterization of a single-molecule DNA switch in free solution. *J Am Chem Soc* 128:11423–11432.
6. Chadborn N, Bryant J, Bain AJ, O'Shea P (1999) Ligand-dependent conformational equilibria of serum albumin revealed by tryptophan fluorescence quenching. *Biophys J* 76:2198–2207.
7. Wu P, Brand L (1992) Orientation factor in steady-state and time-resolved resonance energy transfer measurements. *Biochemistry* 31:7939–7947.
8. Haas E, Katchalski-Katzir E, Steinberg IZ (1978) Effect of the orientation of donor and acceptor on the probability of energy transfer involving electronic transitions of mixed polarization. *Biochemistry* 17:5064–5070.
9. Hillger F, et al. (2008) Probing protein-chaperone interactions with single-molecule fluorescence spectroscopy. *Angew Chem Int Ed* 47:6184–6188.
10. Szabo A, Schulten K, Schulten Z (1980) First passage time approach to diffusion-controlled reactions. *J Chem Phys* 72:4350–4357.

11. Friedler A, et al. (2002) A peptide that binds and stabilizes p53 core domain: Chaperone strategy for rescue of oncogenic mutants. *Proc Natl Acad Sci USA* 99:937–942.
12. Haran G, Haas E, Szpikowska BK, Mas MT (1992) Domain motions in phosphoglycerate kinase: Determination of interdomain distance distributions by site-specific labeling and time-resolved fluorescence energy transfer. *Proc Natl Acad Sci USA* 89:11764–11768.

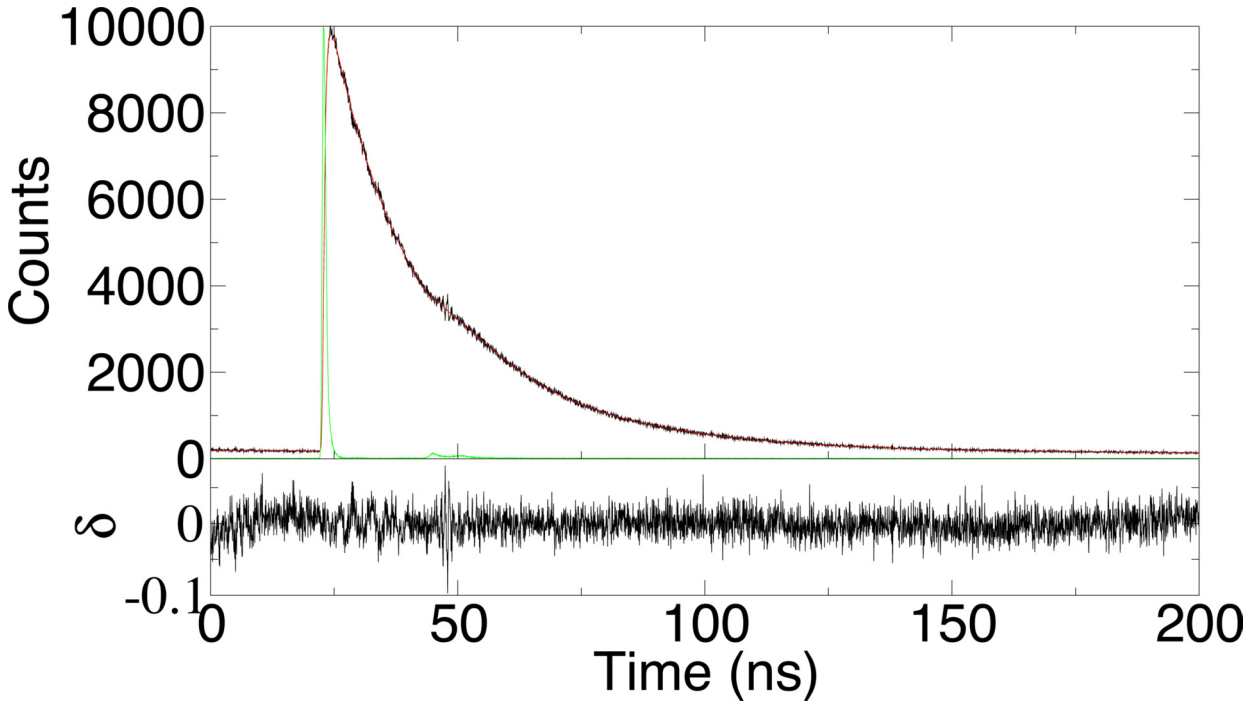

Fig. S1. Time-resolved fluorescence spectrum. Shown are the time-resolved fluorescence (black), the instrument response function (green), deconvoluted fit (red), and the fitting residual (bottom, black).

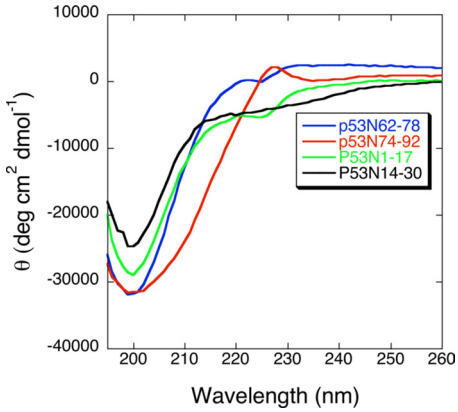

Fig. S2. Circular dichroism spectra for peptides derived from the NTD of p53.

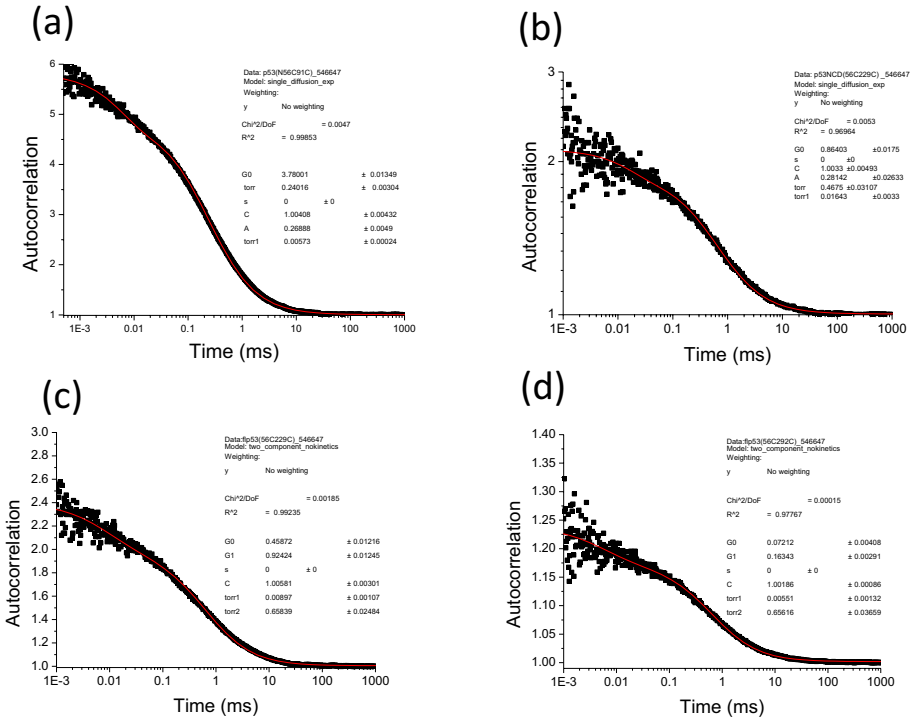

Fig. S3. Typical FCS curves. Shown are the FCS curves for p53N56C91C (*a*), p53NCD56C229C (*b*), flp5356C229C (*c*), and flp5356C292C (*d*), which were fitted by assuming there is a single diffusion component and a fast photophysicsisics process. The experiments confirmed the absence of aggregates.

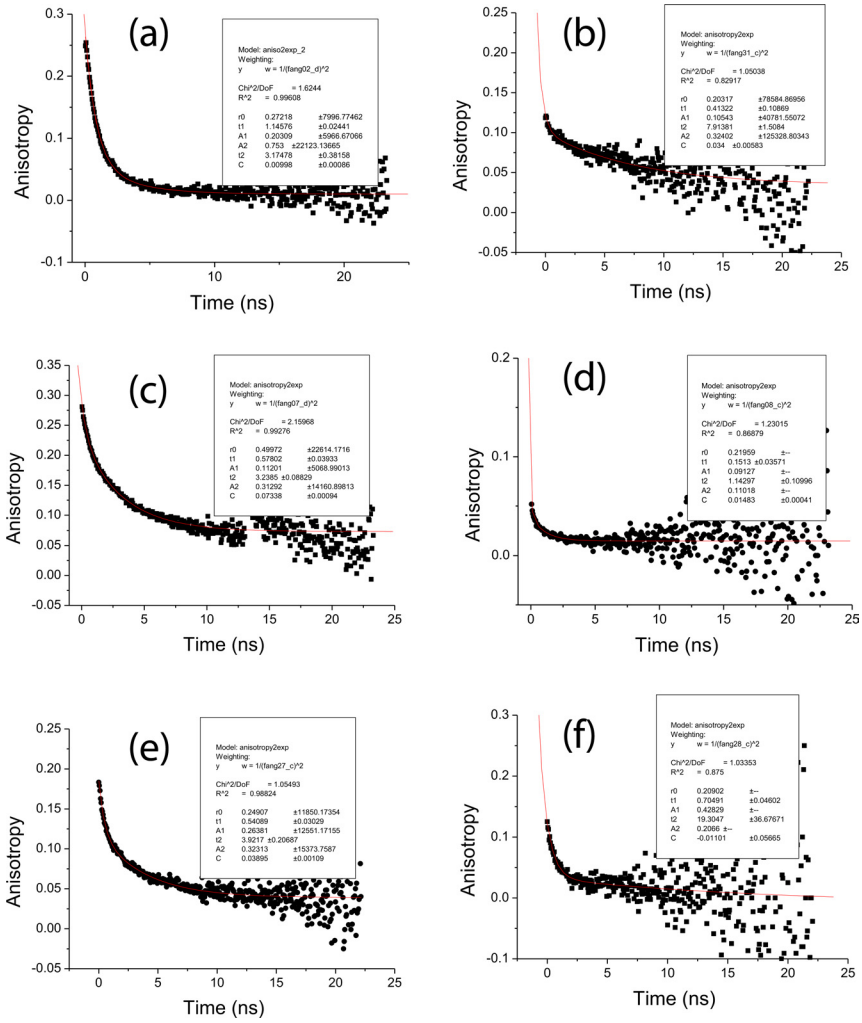

Fig. S4. Typical time-resolved fluorescence anisotropy decay curves. (*a*) flp5356C labeled with AF546 at position 56. (*b*) flp53229C labeled with AF488 at position 229. (*c*) The donor signal for flp5356C292C labeled with both AF546 and AF647. (*d*) The acceptor signal in the presence of FRET for flp5356C292C labeled with both AF546 and AF647. (*e*) The donor signal for flp5356C229C labeled with both AF488 and AF647. (*f*) The acceptor signal in the presence of FRET for flp5356C229C labeled with both AF488 and AF647. The faster relaxation decay is an indication of no restricted fluorophore motions and absence of aggregates.

Table S1. Parameters of the distance distribution, diffusion coefficient, and χ^2 obtained from the fit of TR-FRET data with the program developed by Haas and colleagues (12)

Parameter	p53N1–17	p53N14–30	p53N62–78	p53N74–92
Mean, Å	$22.3^{+3.8}_{-0.3}$	$26.5^{+1.9}_{-0.0}$	$25.5^{+0.8}_{-1.1}$	$24.4^{+0.4}_{-0.5}$
Standard deviation, Å	$5.4^{+10.8}_{-0.0}$	$11.1^{+2.1}_{-0.6}$	$10.9^{+0.5}_{-1.7}$	$7.2^{+0.0}_{-1.1}$
Diffusion coefficient, Å²/ns	0.3–1	0–2.9	0–0.3	0–0.1
χ^2	1.423	1.148	1.271	1.297